The early dendritic cell signaling induced by virulent Francisella tularensis strain occurs in phases and involves the activation of ERKs and p38 in the later stage

Fabrik, Ivo; ...; ...; ...; ...; ...; ...; ...; ...; ...; ...

MCP Papers in Press. Published on October 18, 2017 as Manuscript RA117.000160

The early dendritic cell signaling induced by virulent *Francisella tularensis* strain occurs in phases and involves the activation of ERKs and p38 in the later stage.

Ivo Fabrik[1], Marek Link[1], Daniela Putzova[1], Lenka Plzakova[1], Zuzana Lubovska[2], Vlada Philimonenko[2,3], Ivona Pavkova[1], Pavel Rehulka[1], Zuzana Krocova[1], Pavel Hozak[2,3], Marina Santic[4], and Jiri Stulik[1]*

[1] Department of Molecular Pathology and Biology, Faculty of Military Health Sciences, University of Defence, 500 01 Hradec Kralove, Czech Republic

[2] Institute of Molecular Genetics ASCR v.v.i., Microscopy Centre, Electron Microscopy Core Facility, 142 20 Prague 4, Czech Republic

[3] Institute of Molecular Genetics ASCR v.v.i., Department of Biology of the Cell Nucleus, 142 20 Prague 4, Czech Republic

[4] Department of Microbiology, Faculty of Medicine, University of Rijeka, 51000 Rijeka, Croatia

* To whom correspondence should be addressed: jiri.stulik@unob.cz; phone: 00420 973 253 220; fax: 00420 495 513 018

Running title: Dendritic cell signaling induced by *F. tularensis*

Abbreviations

AMPK	AMP-activated protein kinase
AP-1	activator protein 1
BMDC	bone marrow-derived dendritic cell
CREB	cAMP-responsive element-binding protein
DC	dendritic cell
ERK	extracellular signal–regulated kinase
GAP	GTPase-activating protein
GEF	guanine nucleotide exchange factor
GM-CSF	granulocyte-macrophage colony-stimulating factor
GSK	glycogen synthase kinase
HILIC	hydrophilic interaction chromatography
IFN-β	interferon-β
IKK	inhibitor of NF-κB kinase
JNK	c-Jun N-terminal kinase
LPS	lipopolysaccharide
MAPK	mitogen-activated protein kinase

MAPKAPK	MAPK-activated protein kinase
MOI	multiplicity of infection
mTOR	mammalian target of rapamycin
NF-κB	nuclear factor κ-light-chain-enhancer of activated B cells
p70S6K	p70 ribosomal S6 kinase
PAK	p21-activated kinase
PI3K	phosphoinositide 3-kinase
RSK	p90 ribosomal protein S6 kinase
SILAC	stable isotope labeling by amino acids in cell culture
TLR	toll-like receptor

Summary

Dendritic cells (DCs) infected by *Francisella tularensis* are poorly activated and do not undergo classical maturation process. While reasons of such unresponsiveness are not fully understood, their impact on the priming of immunity is well appreciated. Previous attempts to explain the behavior of *Francisella*-infected DCs were hypothesis-driven and focused on events at later stages of infection. Here, we took an alternative unbiased approach by applying methods of global phosphoproteomics to analyze the dynamics of cell signaling in primary DCs during the first hour of infection by *Francisella tularensis*. Presented results show that the early response of DCs to *Francisella* occurs in phases and that ERK and p38 signaling modules induced at the later stage are differentially regulated by virulent and attenuated Δ*dsbA* strain. These findings imply that the temporal orchestration of host pro-inflammatory pathways represents the integral part of *Francisella* life-cycle inside hijacked DCs.

Introduction

Francisella tularensis is a Gram-negative bacterium and intracellular pathogen that is responsible for tularemia disease (1). Although humans are not the primary hosts, *Francisella* capacity to cause respiratory infections with the relatively high mortality rates prompted the classification of the bacterium as a potential biological weapon (2). The disease itself is characterized by the delayed onset of the adaptive immunity which is then followed by the hypercytokinemia (3). The sub-optimal host response comes as a consequence of *Francisella* ability to avoid the activation of phagocytes in which the bacterium replicates (4). *Francisella* initiates its intracellular life cycle by the entry into the host cell where it transiently resides within the phagosome. Following 30-60 minutes post infection (p.i.), *Francisella* escapes from the vacuole into the host cell cytosol and it replicates there (5). Dendritic cells (DCs), as professional phagocytes, are also susceptible to *Francisella* infection. In similar to the situation in other host cells, *Francisella*-infected DCs are not sufficiently stimulated, do not produce pro-inflammatory cytokines and do not undergo the classical process of maturation (6). Consequently, these DCs have only a limited capacity to prime the adaptive response and they serve rather as migrating bacterial reservoirs. The weak immunostimulatory phenotype of infected DCs correlates with *Francisella* tendency to evade the host pro-inflammatory signaling. *Francisella*-mediated activation of nuclear factor κ-light-chain-enhancer of activated B cells (NF-κB) is dependent on toll-like receptor 2 (TLR2)/myeloid differentiation primary response protein 88 (MyD88) stimulation (7). However, the bacterium is able to reduce the NF-κB-driven gene expression either through the modulation of phosphoinositide 3-kinase (PI3K)/Akt pathway or by the rapid escape from the phagosome (7, 8). In cytosol, the sensing of *Francisella* DNA triggers stimulator of interferon genes (STING)-dependent type I interferon (IFN) response

which helps to orchestrate the inflammasome assembly and caspase 1 activation (9, 10). Nevertheless, although virulent *Francisella* stimulates in DCs the expression of IFN-β, the pyroptosis is suppressed (11). *Francisella* manipulation of DC response therefore evolves in time and follows the bacterial needs. From this perspective, the early *Francisella*-DC interactions represent the crucial phase which directs the future events of DC activation and potentially shapes the adaptive immune response.

To better understand these early processes, we analyzed the cell signaling dynamics of primary DC during the first hour of *Francisella* infection by SILAC (stable isotope labeling by amino acids in cell culture) based phosphoproteomic approach. Our results reveal the existence of distinct phases of protein phosphorylation in infected DCs. While the initial stage seems to be connected with the general process of the bacterial entry, the induction of extracellular signal–regulated kinase (ERK) and p38 signaling during the later phase is regulated differently by the used virulent and attenuated *Francisella* strains.

Experimental procedures

Cultivation of bacteria

All *Francisella tularensis* strains were cultured on McLeod agar enriched for bovine hemoglobin and Iso-Vitalex (both Becton Dickinson) at 37 °C.

Generation/SILAC labeling of bone marrow-derived DCs (BMDCs) and J774.2 cultivation

BMDCs were generated from bone marrow progenitors isolated from femurs and tibias of 6- to 8-week-old female C57BL/6 mice. Approximately 1×10^7 bone marrow cells were seeded on 10 cm tissue plastic Petri dish into 10 mL of RPMI-1640 media containing 10% (v/v) fetal bovine serum (FBS; Sigma Aldrich) and penicillin/streptomycin and these were left at 37 °C in a humidified atmosphere of 5% CO_2. After overnight depletion of adherent cells, suspension cells were seeded on a new dish in RPMI-1640, 10% FBS, and 5% (v/v) supernatant from Ag8653 cells transfected by cDNA of murine granulocyte-macrophage colony-stimulating factor (GM-CSF). Cells were passaged every 2−3 days. Suspension cells were harvested on the day 9 of cultivation. SILAC labeling of BMDCs was performed as previously described (12). All experiments using mice were performed in accordance with guidelines of the Animal Care and Use Ethical Committee of the Faculty of Military Heath Sciences, University of Defense, Czech Republic (project no. 50-6/2016-684800). The murine macrophage-like cell line J774.2 was obtained from the European Collection of Cell Culture (EACC, ref No. 85011428). J774.2 were cultured in high glucose DMEM containing 10% (v/v) FBS (Sigma Aldrich) and kept at 37 °C in a humidified atmosphere of 5% CO_2. Cells were passaged every 2-3 days.

Infections and treatments

Unless otherwise noted, all infection experiments were done as described: harvested BMDCs were seeded into fresh RPMI-1640 medium containing 10% FBS (or SILAC medium with 10% dialyzed FBS in the case of proteomics experiments) at 2.5×10^6 cells/ml. Infection was initiated by the addition of bacteria suspended in the medium of the same composition followed by thorough mixing. Multiplicity of infection (MOI) was 50. Infected cells were kept at 37 °C/5% CO_2 and the infection was stopped by the addition of excess of ice-cold PBS followed by centrifugation of suspension at 4 °C. For 24 h infection intervals, BMDCs were seeded at 2×10^6 cells/ml and MOI was 10. Cells treated by *E. coli* 055:B5 lipopolysaccharide (LPS; 500 ng/ml) were used as a positive control. In experiments with killed *Francisella*, bacteria were first fixed by 3.7% (w/v) paraformaldehyde (PFA) at 4 °C overnight and then used as an infection agent at apparent MOI 100. For synchronization of BMDC infection, bacterial suspension was mixed with the suspension of 7.5×10^6 cells (MOI 50) in flat-bottom falcon tube and immediately co-pelleted in centrifuge (400 g, 5 min, RT). Following the centrifugation (t = 0), cells were kept at 37 °C/5% CO_2 for the indicated time p.i. Mock-infected BMDCs were centrifuged without bacteria. When indicated, seeded BMDCs were pre-treated either by DMSO or by bafilomycin A1 or SB203580 (both Sigma Aldrich) for 1 hour at final concentrations of 100 nM or 10 μM, respectively, followed by the addition of bacteria. DMSO/inhibitors were present in the medium throughout the infection. Adherent J774.2 cells were infected in 6-well plates (1×10^6 cells/well) by co-centrifugation (400g, 5 min, RT) with bacteria (MOI 50) and left for 60 min at 37 °C/5% CO_2.

Cell lysis and protein digestion

BMDC pellets were lysed by sodium deoxycholate (SDC)-containing buffer as previously described (13). Protein concentrations were measured using the Micro BCA kit (Thermo Pierce)

and the corresponding light and heavy isotope-labeled lysates were mixed in a 1:1 ratio based on protein content. Proteins were reduced by the addition of DTT (final concentration 10 mM) for 1 h at 37 °C, followed by the alkylation with iodoacetamide (IAA; final concentration 20 mM) for 30 min at room temperature in the dark. The excess of IAA was quenched by the addition of DTT to a final concentration of 20 mM and the reaction was left to proceed for 15 min at room temperature. Proteins were digested by trypsin (Promega) at a ratio 50:1 (w/w) at 37 °C overnight. Digestion was stopped by the addition of TFA to a final concentration of 1% (v/v) to precipitate SDC. Suspension was then mixed with an equal volume of ethyl acetate, vortexed and centrifuged. Upper organic phase was removed and the extraction process was repeated four times to completely extract SDC (14). Water phase containing peptides was then desalted on Discovery DSC-18 SPE cartridges (500 mg/3 mL; Sigma Aldrich) and the eluate in 80% ACN/0.1% TFA was vacuum dried.

HPLC fractionation

Fractionation of peptides was done using Alliance 2695 liquid chromatograph (Waters). For phosphoproteome analysis, BMDC digests were fractionated by hydrophilic interaction chromatography (HILIC) (15). Peptide material of 3 to 5 mg was injected onto TSKgel Amide-80 HR column (5 µm, 4.6 × 250 mm) with guard column (5 µm, 4.6 × 10 mm; both Tosoh Bioscience) under conditions of 20% mobile phase A (2% ACN/0.1% TFA) and 80% mobile phase B (98% ACN/0.1% TFA) at flow rate of 0.5 mL/min. Peptide separation was performed by a linear gradient formed by mobile phase A and mobile phase B, from 80 to 60% of mobile phase B in 40 min and from 60 to 0% of mobile phase B in 5 min. Through the gradient elution window, 20 fractions were manually collected into microcentrifuge tubes. For analysis of BMDC proteome at 60 min p.i., 200−300 µg of peptides were fractionated by high-pH reversed phase

liquid chromatography as previously described (16) and 10 fractions were manually collected through the gradient elution window. Prior LC-MS analysis, fractions 1 and 2 were pooled with fractions 9 and 10, respectively.

Phosphopeptide enrichment

Collected HILIC fractions were first acidified by 2% (v/v) TFA solution containing 100 mM glutamic acid as an excluder, followed by the addition of 1.5−2.5 mg of TiO_2 particles (10 µm, GL Sciences). Suspensions were then vortexed for 20 min at room temperature and centrifuged. Pellets of TiO_2 were sequentially washed in buffers A (65% ACN/2% TFA/100 mM glutamic acid), B (65% ACN/0.5% TFA), and C (65% ACN/0.1% TFA). TiO_2-bonded phosphopeptides were eluted by vortexing particles for 10 min at room temperature in ammonia solution (pH ≈ 11) followed by the acidification of supernatants by TFA to reach pH 2. Each HILIC fraction was subjected to two identical cycles of the enrichment and TiO_2-eluates from the same fraction were pooled, desalted on 3M Empore SPE cartridges (Sigma Aldrich) and the eluates in 65% MeOH/0.1% TFA were vacuum-dried.

Liquid chromatography-mass spectrometry

The Ultimate 3000 RSLCnano system connected through Nanospray Flex ion source with Q Exactive mass spectrometer (Thermo Scientific) were used for instrumental analysis (17). For phosphoproteome analysis, approximately one third of sample material from each phosphopeptide fraction was introduced onto trap column (PepMap100 C18, 3 µm, 0.075 × 20 mm) and then separated by running a linear gradient (0.1% FA in water as phase A; 80% ACN, 20% water and 0.1% FA as phase B) from 4 to 34% B in 48 min and from 34 to 55% B in 10 min, at a flow rate of 300 nL/min, on analytical column (PepMap C18, 2 µm, 0.075 × 150 mm).

The full MS/Top10 setup was used for mass spectra acquisition. The positive ion MS spectra from 350-1750 m/z range were obtained in the Orbitrap at a resolution of 70,000 (at m/z 200). Multiply charged precursors ions with minimal threshold intensity of 5×10^4 counts and not fragmented during previous 30 s were admitted for higher energy collisional dissociation (HCD). Tandem mass spectra were acquired with following settings; resolution at 17,500, AGC target value at 1×10^5, maximum ion injection time at 100 ms, and normalized collision energy set to 27. Data acquisition was under control of Xcalibur software v3.0. Proteome samples fractions were analyzed by the same instrumentation using a linear gradient from 4 to 30% B in 88 min and from 30 to 55% B in 25 min for separation. Mass spectrometer operated in Top12 setup and collected MS spectra were in range of 350-1650 m/z. Intensity threshold for triggering MS/MS was 6×10^4 counts. The rest of instrumental parameters were identical to those of phosphoproteome analysis.

Phosphosite and protein identification and quantification

Phosphoproteome and proteome datasets were processed by MaxQuant ver. 1.5.2.8 coupled with Andromeda search engine (18). Data were searched against FASTA database consisting of reference proteome for *Mus musculus* (UP000000589; June 16, 2015; 53,245 sequences) and Swiss-Prot + TrEMBL database entry for *Francisella tularensis* subsp. *holartica* FSC200 strain (January 27, 2015; 1424 sequences), both downloaded from Uniprot site. MaxQuant-implemented database was used for the identification of contaminants. False discovery rate (FDR) estimation of peptide identification was based on target-decoy approach using reverted search database as a decoy. Phosphosite identification and quantification was done using these MaxQuant parameters: mass tolerance for the first search 20 ppm, for the second search from recalibrated spectra 4.5 ppm (with individual mass error filtering enabled); maximum of 2

missed cleavages; maximal charge per peptide z = 7; minimal length of peptide 7 amino acids, maximal mass of peptide 4600 Da; carbamidomethylation (C) as fixed and phosphorylation (STY), oxidation (M) and acetylation (protein N-term) as variable modifications with the maximum number of variable modifications per peptide set to 5. Trypsin with no cleavage restriction was set as a protease. Mass tolerance for fragments in MS/MS was 20 ppm, taking the 12 most intensive peaks per 100 Da for search (with enabled possibility of co-fragmented peptide identification). Minimal Andromeda score for modified peptides was 40 and minimal delta score for modified peptides was 6. FDR filtering on peptide spectrum match was 0.01 with separate FDR filtering for each modification set to 0.01. For peptide quantitation, Arg+6 [$^{13}C_6$] and Lys+6 [$^{13}C_6$] were set as labels in heavy channel (or in light channel for label-swap experiments to obtain inverted H/L ratios) with re-quantify function enabled. Ratios for individual phosphosites were derived from normalized ratios of the least modified phosphopeptides in a given replicate. MaxQuant parameters for processing of proteome data were identical except for only oxidation (M) and acetylation (protein N-term) were allowed as variable modifications. For protein quantitation, only protein groups with at least one unique or razor peptide having SILAC ratio and only those protein groups passing protein FDR filtering set to 0.01 were considered (18). All hits identified in searches as contaminants were filtered out.

Experimental design and statistical rationale

SILAC experiments were performed in biological triplicate for each time point and bacterial strain used and the respective mock-treated BMDCs served as a control. In two replicates, light BMDCs were infected and heavy cells were mock-treated. In one replicate, SILAC groups were swapped (Fig. S1). In total, 18 digests (three time points/two bacterial strains/triplicate) were fractionated by HILIC. Aliquots of 6 digests (60 min p.i./two bacterial strains/triplicate) were

also subjected to proteome analysis. Significantly regulated phosphosites for each triplicate (time point/bacterial strain) were found by global mean rank test (GMRT) (19) using R package MeanRankTest (https://www.evotec.com/MeanRankTest) with parametric FDR level set to 0.05. Only those phosphosites quantified in all three replicates of the given experimental condition were allowed for testing. With respect to the obtained phosphoproteomic data, GMRT was chosen for two reasons: i) rank tests in general are advantageous for global methods when fold changes are relatively low (20) and ii) GMRT was shown to reliably control FDR even for small number of replicates (19).

Phosphosite fuzzy *c*-means clustering

Fuzzy *c*-means clustering (21) of phosphosites with localization probability >0.75 (22, 23), which were quantified in all three time points for WT-infected BMDC samples with the relative standard deviation (RSD) <30%, was done by *Mfuzz* R package (24). For a given phosphosite, normalized $\log_2$-ratios from replicates were first averaged and multiplied by -1 for each time point and then normalized by Z-score. Fuzzifier was set to 3.65 (25) and the number of clusters was 4. Human protein reference database (HPRD) (26) kinase motifs enriched in phosphosite clusters were found by Fisher exact test (Benjamini-Hochberg (BH) FDR level set to 0.05) using Perseus software ver. 1.5.4.1 (27).

InnateDB terms enrichment and the construction of protein-protein interaction network

For the comparison of BMDC response induced by WT and Δ*dsbA Francisella* strains, normalized $\log_2$-ratios of phosphosites quantified in all three replicates of WT-infected BMDCs samples were tested by unpaired two sample Student's t test against those quantified in all three replicates of Δ*dsbA*-infected BMDCs samples of the same time interval. Phosphosites (and

corresponding phosphoproteins) having p <0.05 were further considered as differentially regulated between BMDCs infected by WT and Δ*dsbA*. For InnateDB term analysis, phosphoproteins were first annotated by Pathway analysis web-based tool from InnateDB database (http://www.innatedb.com/) (28) and Fisher exact test was then used to find enriched InnateDB Pathway name terms in the group of differentially regulated phosphosites (BH FDR level set to 0.05). Only terms containing at least 3 regulated phosphosites are reported. In case where the same group of phosphosites was annotated by several similar enriched InnateDB terms, one representative term was selected. Using the described approach, none InnateDB terms were found enriched for 10 and 30 min p.i. For the construction of protein-protein interaction network, only proteins bearing phosphosites differentially regulated between WT- and Δ*dsbA*-infected BMDCs at 60 min p.i. were considered. Sequences were mapped to murine protein sequences on STRING (v10) (29) using BLAST to obtain database identifiers and best matches with at least 80% identity were used. STRING interaction network containing interactions with >700 score was then loaded into Cytoscape ver 3.2.1 and only differentially regulated phosphoproteins or proteins having at least two differentially regulated neighbors ("connecting" nodes) were kept. The emerging network was then reduced to contain smallest possible number of "connecting" nodes while keeping all regulated phosphoproteins in one network (i.e. removing "connecting" nodes with relatively low number of neighbors). In cases where could not be decided, all equivalent nodes were kept.

Immunofluorescence microscopy

Bacteria were incubated for 1 h with 5 μM 5-(and 6)-carboxyfluorescein diacetate succinimidyl ester (CFDA-SE) prior the infection. BMDCs were then infected as described in Experimental procedures, transferred to glass slide using cytospin and fixed by 3.7% PFA. The excess of PFA

was quenched by 50 mM NH_4Cl and cells were permeabilized by 50 µg/ml digitonin for 1 min. BMDCs were then stained for 20 min by Alexa Fluor 594 Phalloidin (6.6 µM) and for 5 min by 4',6-diamidino-2-phenylindole (DAPI, 300 nM) and mounted by Mowiol. Microscope slides were viewed by fluorescence microscopy on Nikon Eclipse Ti (Nikon, Tokyo, Japan). Percentage of infected cells was calculated as an average of 500 cross-sectional images per time point.

Transmission electron microscopy

Infected of uninfected cells were quickly washed with Sörensen buffer (0.1 M sodium/potassium phosphate buffer, pH 7.3; SB) at 37 °C, fixed with 2.5% glutaraldehyde in SB for 2 h, washed with SB, embedded in blocks of 1% low-melting point agarose (type VII, Sigma Aldrich), and postfixed with 1% OsO_4 solution in SB for 2 h. The cells were dehydrated in series of ethanol with increasing concentration, subsequently in propyleneoxide, and embedded in Epon-Durcupan resin. Polymerized blocks were cut into 80 nm ultrathin sections, collected on 200 mesh size copper grids, and stained with saturated aqueous solution of uranyl acetate for 4 min. The sections were examined in FEI Morgagni 268 transmission electron microscope operated at 80 kV. The images were captured using Mega View III CCD camera (Olympus Soft Imaging Solutions).

Flow cytometry

Following 24 h of infection, suspension BMDCs were harvested and stained by following antibodies: anti-CD11c-phycoerythrin (PE)-Cy7 (BD Pharmingen), anti-CD80-PE (Beckman Coulter), anti-CD86-PE (Beckman Coulter), and anti-I-A/I-E major histocompatibility complex II (MHC II) conjugated with biotin (Novus Biologicals), respectively. Anti-MHC II antibodies

were then stained by streptavidin-FITC (Invitrogen). Cells were fixed and before analysis on CyAn ADP flow cytometer (Beckman Coulter) stained by propidium iodide. Data acquisition and interpretation were done using Summit 4.3 software (Beckman Coulter).

ELISA

Quantification of cytokines in cell culture supernatants was done using DuoSet ELISA kits (R&D Systems) according to manufacturer instructions.

Quantitative real-time PCR

RNA was isolated from cells using RNeasy kit from Qiagen. 1 µg of total RNA was reverse transcribed using oligo (dT) primers (New England Biolabs). Quantitative real-time PCR analysis was performed and analyzed using ABI Prism 7500 Fast RT-PCR System (Applied Biosystems). Data were normalized to the housekeeping gene 18S rRNA (*Rn18S1*) and expressed as fold change relative to RNA samples from mock-treated cells using the comparative Ct method (ΔΔCt). The following TaqMan Gene Expression Assays were used (Applied Biosystems): *Il10* (Mm01288386_m1), *Il12b* (Mm01288989_m1), *Ifnb1* (Mm00439552_s1), and *Rn18S1* (Mm03928990_g1).

Western blot

Cell pellets were lysed in RIPA buffer containing protease (Roche) and phosphatase (cocktail set II, Merck) inhibitors. Denatured and reduced proteins were separated by SDS-PAGE and transferred to PVDF membranes. Blots were blocked by milk and incubated with primary antibody overnight followed by secondary antibody conjugated with horse-radish peroxidase (Dako). Bands were visualized by ECL (Amersham). Anti-β-actin and anti-tubulin antibodies

were purchased from Sigma Aldrich and Abcam, respectively. The rest of primary antibodies were obtained from Cell Signaling.

Results

Francisella induces two waves of protein phosphorylation in BMDCs during the first hour of infection

SILAC-labeled primary murine bone marrow-derived DCs (BMDCs) (12) were infected by fully virulent *Francisella tularensis* subsp. *holarctica* FSC200 strain (WT) in suspension without the synchronization by centrifugation to avoid TLR2-MyD88-dependent NF-κB activation caused by a mechanical force (30). BMDCs were lysed at 10, 30, and 60 min p.i. and the lysates were processed and analyzed as described in Experimental procedures (Fig. S1). In total, 17,535 phosphosites from *Francisella*-infected BMDC proteome were identified. From these, more than 5,000 were quantified in all replicates of each experimental condition (time/bacterial strain; Fig. S2 and Table S1). In general, *Francisella*-induced phosphorylation events in BMDCs were most apparent at 10 min p.i. (Fig. 1A). Consistently, the highest number of phosphosites was classified as significantly regulated at 10 min p.i. (Fig. 1B and Fig. S3). Surprisingly, following the drop at 30 min p.i., there was a new increase in BMDC protein phosphorylation at 60 min p.i. This observation was not caused artificially by the variability of data. Phosphoproteome samples were grouped together according to the time p.i. in PCA (Fig. S4A). Although the relatively small phosphorylation changes and sub-optimal SILAC labeling efficiency of primary BMDCs (12) led to the low correlation of label swap replicates, there was no difference between 30 and 60 min p.i. datasets in terms of the distribution of RSDs for phosphosites SILAC ratios (Fig. S4B). The increase in BMDC signaling at 60 min p.i. was also not affected by the changes in protein expression or degradation (Fig. S5). To further analyze phosphorylation dynamics in infected BMDCs, fuzzy *c*-means clustering was used to group reproducibly quantified phosphosites according to their time profiles (Fig. 1C and 1D). In line with results shown in Fig. 1B, cluster

peaking at 10 min p.i. (cluster A) contained the highest number of phosphosites (Fig. 1C). To identify potentially involved kinases, clustered phosphosites were searched for Human Protein Reference Database (HPRD) kinase motifs (Table 1) and prevalent sequence features were assembled for each cluster. Activities of several kinases seemed to follow the profile of the largest phosphosite cluster A; e.g. p70 ribosomal S6 kinase (p70S6K), Akt or p21-activated kinase 2 (PAK2) (Table 1). Importantly, activities of these kinases were confirmed by Western blot (Fig. 1E). The large part of phosphoproteins regulated at 10 min p.i. was functionally linked to regulation of cytoskeleton and vesicular transport (Table S1). Among them, GTPase-activating proteins (GAPs) and guanine nucleotide exchange factors (GEFs) of Rac and Cdc42 GTPases (e.g. Arhgaps, Arhgefs or Docks) represented the most notable examples. GEFs activate Rac/Cdc42 and promote their binding to PAKs, which in turn stimulates PAK autophosphorylation and activation. Such autophosphorylation of PAK1 (S204) and PAK2 (S55 and S197) was indeed detected at 10 min p.i., therefore indirectly confirming previous kinase motif analysis (Fig. 1D, 1E and Table 1) and supporting the active role of Rho GTPase-PAK signaling in *Francisella* internalization. In contrast to 10 min p.i., only few potential kinases could be associated with the second signaling maximum occurring 60 min p.i. (clusters B and D in Fig. 1D and Table 1, respectively). While the activity of AMP-activated protein kinase (AMPK) gradually increased and peaked at 60 min p.i. (cluster D in Fig. 1D and Fig. 1E), ERKs displayed more complex behavior as their kinase motif was enriched in phosphosite cluster displaying maxima at 10 min and 60 min p.i. (cluster B in Fig. 1D).

***Francisella* mutant lacking *dsbA* gene may serve as an avirulent control to WT strain in BMDCs**

The identification of DC signaling pathways regulated in response to *Francisella* virulent behavior could be facilitated by the confrontation of results with experiments where attenuated strain was used as a control. *Francisella* strains lacking *dsbA* gene (Δ*dsbA*) are attenuated *in vivo* and provide the protection against subsequent challenge by parental strain (31–33). The engagement of adaptive immunity suggests that Δ*dsbA* would represent suitable alternative to WT in terms of DC response. To assess *in vitro* ability of Δ*dsbA* to induce BMDC maturation, cells were infected by FSC200 WT and Δ*dsbA* mutant of the same background and surface expression of MHC II, CD80 and CD86 was measured 24 h p.i. by flow cytometry (Fig. 2A). For all presented maturation markers, Δ*dsbA*-infected BMDCs showed higher expressions than cells infected by WT. Similarly, *in vitro* secretion of pro-inflammatory cytokines IL-12p40, IL-1β and IL-6 was higher in BMDCs infected by Δ*dsbA* at 24 h p.i. (Fig. 2B). The observed differences between strains were not skewed by BMDC cell death (Fig. S6A). Note however, that both WT and Δ*dsbA* strains were relatively poor inducers of BMDC cytokine secretion compared to *Francisella* Live Vaccine Strain (LVS; Fig. 2B). Moreover, the viability of cells in general (Fig. S6A) might further affect the cytokine production since the levels of IL-12p40 secreted by Δ*dsbA*-infected BMDCs did not exceed those of uninfected cells and the production in WT-infected BMDCs was even lower (Fig. 2B). Consistently, the levels of IL-12p70 and IL-23 secreted by BMDCs infected with either WT or Δ*dsbA* were below the level of detection. To explore the intracellular fate of bacterial strains, WT- and Δ*dsbA*-infected BMDCs were subjected to transmission electron microscopy at 60 min p.i. Similarly to what was previously reported (34), WT bacteria were located primarily in the cytosol at this time p.i. (Fig. 2C). In contrast, the majority of Δ*dsbA* bacteria (~60%) were surrounded by the damaged vacuolar membrane (Fig. 2C) which suggested the intracellular trafficking of Δ*dsbA* in BMDCs differed

from that of virulent strain. Importantly, while the unsynchronized infection reduced BMDC infectivity, the dynamics of WT and Δ*dsbA* host entry did not differ significantly (Fig. S6B). Taken together, the results confirmed the attenuated nature of Δ*dsbA* in BMDCs *in vitro* and encouraged its use as an avirulent control for phosphoproteomics experiments where WT was an infection agent (Fig. S1).

Signaling of mTOR/p70S6K is sustained 60 min p.i. in WT-infected BMDCs

BMDCs infected by Δ*dsbA* mutant were processed and analyzed for phosphoproteome changes exactly as for WT-treated cells. Dominant feature of WT-infected BMDCs was an early Akt activation (see above) (8). To examine whether WT and Δ*dsbA* mutant differed in their ability to trigger Akt signaling, time profiles of several identified Akt targets phosphorylated in both WT- and Δ*dsbA*-infected BMDCs at 10 min p.i. were compared (Fig. 3A, Table S1). Phosphorylation trends of Tuberin (Tsc2; T1465), proline-rich AKT1 substrate 1 (PRAS40; T247), glycogen synthase kinase-3 β (GSK-3β; S9) or AMPK α1 (S496) followed the predicted Akt activity (cluster A in Fig. 1D) similarly in both WT- and Δ*dsbA*-infected BMDCs. Importantly, these proteins are responsible for the suppression of mammalian target of rapamycin complex 1 (mTORC1) activity and Akt-mediated phosphorylation release mTORC1 from their inhibition (35–38). This suggested that mTOR activity should follow that of Akt in both WT- and Δ*dsbA*-infected BMDCs (Fig. 1D). However, several phosphosites associated with mTOR signaling were found to be upregulated at 60 min p.i. in BMDCs infected by WT (Fig. 3B, Table S1). While phosphorylation of mTOR on S1261 was shown to be crucial for the induction of mTORC1 activity (39), functional roles of phosphosites S278 on SH3 domain-binding protein 4 (SH3BP4) and S381 on RagC are unknown. Interestingly, SH3BP4 negatively regulates mTORC1 activity on lysosome lumen through binding of Rag complex via SH3BP4 region

containing S278 (40). Differential regulation of mTOR between WT- and Δ*dsbA*-infected BMDCs at 60 min p.i. was confirmed by Western blot (Fig. 3C). Independently of the bacterial strain used, PRAS40 (T247) phosphorylation (compare with Fig. 3A) and mTOR/p70S6K signaling were induced 10 min p.i. However, mTOR/p70S6K crosstalk at 60 min p.i. was preserved only in WT-infected BMDCs. These results suggest that in contrast to BMDCs infected by Δ*dsbA*, mTOR/p70S6K signaling is maintained in WT-infected BMDCs at 60 min p.i. and that this activity is Akt-independent.

Cell signaling of BMDCs infected by WT and Δ*dsbA* starts to diverge at 60 min p.i.

Observed differences in mTOR activity prompted further inspection of phosphoproteomic data to search for system-wide variations in WT- and Δ*dsbA*-induced BMDC signaling. To determine correlations in phosphoproteomes, phosphosites quantified in the given time point p.i. in both WT- and Δ*dsbA*-infected BMDCs were plotted against each other in scatter plots (Fig. 4A). Phosphorylation changes induced by WT and Δ*dsbA* invasion at 10 min p.i. correlated well. However, WT-infected BMDCs showed more prominent protein phosphorylation with increasing time p.i. (Fig. 4A). This behavior affected also counts of regulated phosphosites (Fig. S3 and Table S1). While at 10 min p.i. the numbers of significantly regulated phosphosites in BMDCs infected by WT and Δ*dsbA* were comparable, almost three times more phosphosites from WT-infected cells passed the significance test when compared to Δ*dsbA* at 60 min p.i. (Fig. S3). Similarly, the numbers of phosphosites, which were considered as differentially regulated between WT- and Δ*dsbA*-infected BMDCs (see Experimental procedures), were almost two times higher at 60 min p.i. (125 sites) than those at 10 or 30 min p.i. (70 and 56, respectively; Fig. S7). Interestingly, the weak correlation of strain-specific signaling temporally corresponded to the second wave of protein phosphorylation at 60 min p.i. in WT-infected BMDCs (Fig. 1B).

BMDC signaling pathways engaged differentially by WT and Δ*dsbA* at 60 min p.i. were found by InnateDB terms enrichment analysis (Fig. 4B). Taken together, WT and Δ*dsbA* induce similar patterns of protein phosphorylation in BMDCs during the entry. BMDC cell signaling start to diverge in later time points p.i. and this is largely due to activation of TLR- and mitogen-activated protein kinase (MAPK)-related pathways in WT-infected cells.

ERKs and p38 modules are major components of WT-induced BMDC signaling at 60 min p.i.

To explore phosphoproteins differentially regulated at 60 min p.i. to a greater depth, protein-protein interaction network was constructed (Fig. S8). The assembly of the network was subjected to two requirements: i) the network should contain as many phosphoproteins differentially regulated in WT- and Δ*dsbA*-infected BMDCs at 60 min p.i. as possible and ii) unidentified proteins should also be included to keep the network together (see Experimental procedures). Notably, the center of the network was formed by a cluster of closely interacting nodes corresponding to MAPKs and MAPK-activated protein kinases (MAPKAPKs) (Fig. 5A). The kinetics of phosphorylation for sites with available quantitative data is shown in Fig. 5B. The phosphorylation profiles of ERK2 and p38α in their activation loops (Y185 and T180, respectively) suggested that these MAPKs are activated at 60 min p.i. only in WT-infected BMDCs. Interestingly, while the activation of p38α in WT-infected BMDCs peaked at 60 min p.i., the phosphorylation of ERK2 was upregulated also at 10 min p.i. in both WT- and Δ*dsbA*-infected BMDCs. Of note, the time profile of ERK2-activation phosphosite in WT-infected BMDCs resembled the V-like shaped phosphosite cluster B (Fig. 1D) for which ERKs kinase motif was enriched (Table 1). While not passing the significance level for differential regulation in WT- and Δ*dsbA*-infected BMDCs at 60 min p.i., phosphosite from the activation loop of

ERK1 (Y205) followed the trend of ERK2 (Fig. 5B). These findings confirmed ERKs as participants in both waves of WT-induced signaling in BMDCs during the first hour of the infection. Differential regulation of ERKs and p38 in WT- and Δ*dsbA*-infected BMDCs affected also the phosphorylation state of MAPKAPKs acting downstream (Fig. 5B and 5C). ERK-dependent phosphorylation of p90 ribosomal protein S6 kinases (RSKs) RSK1 and RSK2 (S352 and T365, respectively) plays a crucial role in their activation (41, 42). Similarly, p38-induced phosphorylation of MAP kinase-activated protein kinase 2 (MAPKAPK2 or MK2) site T320 is a part of MK2-activating cascade (43). Downstream of ERKs and p38 lies also mitogen- and stress-activated kinase 2 (Msk2) whose activity is positively regulated by phosphorylation of T687 (44). As expected, all these sites were significantly more phosphorylated in WT-infected BMDCs at 60 min p.i. (Fig. 5B and 5C). Importantly, phosphorylation kinetics paralleled the time profiles of phosphosites in activation loops of the respective upstream MAPK (Fig. 5B). While there was no direct proof of c-Jun N-terminal kinases (JNKs) involvement in WT-induced BMDC signaling at 60 min p.i., the phosphorylation of JNK-interacting protein 3 (JIP3) (45) was differentially regulated in WT- and Δ*dsbA*-infected BMDCs at this time p.i. (Fig. 5C). To confirm SILAC-based results, the activation states of ERKs, p38 and RSK1 were assessed by Western blot (Fig. 5D). In line with phosphoproteomics data, ERKs and RSK1 were activated in both WT- and Δ*dsbA*-infected BMDCs at 10 min p.i. However, in contrast to WT-infected BMDCs, both kinases returned to their near-basal states in Δ*dsbA*-infected cells at 60 min p.i. As expected, the induction of p38 at 60 min p.i. was observed only in BMDCs infected by WT strain (Fig. 5D). The described MAPK activation profiles were not biased by the efficiency or by the synchronization of the infection (Fig. S9). WT-specific induction of ERKs and p38 at 60 min p.i. raised a question whether the altered host signaling could be related to the increased presence of

WT in the cytosol (Fig. 2C). Bafilomycin A1 treatment is employed to block *Francisella* phagosomal escape in host cells (46, 47). However, bafilomycin A1 alone was a potent inducer of p38 in BMDCs (Fig. S10A) which ruled out its use in this case. Nevertheless, BMDCs treated by escape-negative (47) paraformaldehyde (PFA)-killed bacteria showed a similar level of ERK activation as in WT-infected cells and only p38 activity was dependent on the viability of bacteria (Fig. S10B). Altogether, the results indicate that ERKs and p38 and their downstream effectors RSK1, RSK2, Msk2 and MK2 represent major signaling modules specifically induced in WT-infected cells at 60 min p.i. and that the induction of p38 branch requires viable bacteria.

WT-induced p38 signaling regulates the early expression of pro- and anti-inflammatory cytokines in infected BMDCs

The induction of MAPK/MAPKAPK cascades in WT-infected BMDCs suggested that these cells might also mobilize their transcriptional machinery. Indeed, the observation of WT-driven phosphorylation of proteins associated with inhibitor of NF-κB kinase (IKK) signaling indicated the upregulation of gene expression. Tab2 protein, needed for IKKα/β activation, was phosphorylated (S450) in WT-infected BMDCs at 60 min p.i. (Table S1). Similarly, a known substrate of both canonical IKKs and IKK-related kinases (48) – Tank – was phosphorylated on two residues (S107 and S258; Fig. 6A and Table S1, respectively). Finally, IKK targets NF-κB inhibitor-ε (IκB-ε; S18) (Fig. 6A), IκB-α (Fig. 6B) and Abin2 (S147) (Table S1) were found to be phosphorylated in WT-infected BMDCs at 30 min or 60 min p.i., respectively, and these events are known to have a positive impact on NF-κB-dependent gene expression (49, 50). In addition, the transcriptional activity of activator protein 1 (AP-1) was also upregulated in BMDCs infected by WT as inferred from the phosphorylation of Jun (S73) (Fig. 6A). The described situation favored the expression of *Il12b* in WT-infected BMDCs (Fig. 6D) as the gene

transcription is NF-κB- and AP-1-dependent (51, 52). Notably, although the phosphorylation of Jun was p38-independent (Fig. 6C), the expression of *Il12b* relied on p38 activity (Fig. 6E) which suggests that WT-induced p38 might support NF-κB-dependent transcription (53). The early *Il12b* expression, followed by IL-12p40 secretion (1-6 h p.i.; Fig. 6D and Fig. S11), was in contrast to the situation at 24 h p.i., where the levels of IL-12p40 produced by WT-infected BMDCs were below those produced by Δ*dsbA*-infected cells (Fig. 2B and Fig. S11). The nature of the attenuation of IL-12p40 production in WT-infected BMDCs could not be explained on the basis of the presented phosphoproteomic data as these describe the very early moments of the infection. Nevertheless, several lines of evidence suggested that triggering of MAPK/MAPKAPK signaling in WT-infected BMDCs at 60 min p.i. leads to the activation of cyclic cAMP-responsive element-binding protein (CREB) which is responsible for the transcription of genes with immunosuppressive functions (54). First, InnateDB terms connected to events in the nucleus (including "CREB phosphorylation") were found enriched in the group of proteins differentially phosphorylated in WT- and Δ*dsbA*-infected BMDCs at 60 min p.i. (Fig. 4B). Second, although none of CREB phosphosites were identified as regulated in phosphoproteomic screen, CREB represented an interaction hub in MAPK signaling cluster in the constructed protein-protein interaction network (Fig. 5A). CREB-regulated transcription coactivator 2 (TORC2) was phosphorylated in WT-infected BMDCs at 60 min p.i. (Table S1) at -2 position (S612) to calcineurin binding motif (55). Finally, WT-induced MK2 and Msks MAPKAPKs (see above) are able to phosphorylate the regulatory S133 CREB site (56, 57). In line with the latter, CREB was phosphorylated to a greater extent in WT-infected BMDCs at 60 min p.i. (Fig. 6B) in p38-dependent manner (Fig. 6C). Notably, CREB was also phosphorylated at 10 min p.i. in both WT- and Δ*dsbA*-infected BMDCs and the biphasic activation profile in

WT-infected cells implied the participation of either ERKs (Fig. 1D and 5B) and/or Akt (see Discussion) in the process. The activation of CREB in infected macrophages and DCs leads to the expression of anti-inflammatory genes such as *Il10* (54). Consistently with WT-induced CREB phosphorylation, the increase in *Il10* mRNA was more prominent in WT-infected BMDCs (Fig. 6D) and the stable expression relied on p38 activity (Fig. 6E). The dominant position of MAPK-regulated transcription factors in BMDC transcriptional response to WT might seem surprising considering the cytosolic localization of bacteria at 60 min p.i. (Fig. 2C). Indeed, cytosolic *Francisella* is known to induce expression of type I IFN-related genes through the activation of interferon-regulatory factor 3 (IRF3) by TANK-binding kinase 1 (TBK1) in STING-dependent manner (9, 10, 58, 59). The interaction network in Fig. S8 contained group of proteins potentially involved in cytosolic sensing of bacteria (Fig. S12A). However, the cluster was relatively small and both participants identified in phosphoproteomic screen, Tank (Fig. 6A) and Trafd1 (Fig. S12B), were also shown to participate in the regulation of NF-κB activity (Fig. 6B) (48, 60, 61). In line with the inconclusive findings, the expression of *Ifnb1* was low in both WT- and Δ*dsbA*-infected BMDCs when compared to cells infected by LVS (Fig. S12C). Taken together, these results show that signaling cascades responsible for the activation of NF-κB and CREB in BMDCs are stimulated during the first hour of WT infection and the induced early expression of both *Il12b* and *Il10* genes depends on WT-activated p38 signaling.

Discussion

In this work, we explored phosphorylation signaling of DCs during their early (< 1 hour) interactions with either virulent *Francisella tularensis* subsp. *holarctica* FSC200 (WT) or its avirulent Δ*dsbA* mutant. Such events are known to be differentially regulated in host cells infected by virulent and attenuated strains (7, 62–64) and they represent the initial point of divergence in the activation and the immunogenic development of DCs (6). We demonstrate here that virulent *Francisella* triggers two distinct waves of DC protein phosphorylation within the first hour of infection (Fig. 6F). The initial phagocytosis-induced DC response (10 min p.i.) involves Akt-mediated stimulation of mTOR, the activation of ERK-RSK module, and the regulation of Rac/Cdc42 GAPs and GEFs and PAK autophosphorylation. The active role of ERKs and mTOR in *Francisella* internalization was reported before (65, 66), but this is the first study to show the involvement of PAKs in the process. Their function however remains unclear because PAK activation is associated with macropinocytic uptake (67) which is not the primary mechanism of *Francisella* entry into phagocytes (68). The initial DC response induced by the bacterial engulfment rapidly declines at 30 min p.i. The notable exception represents the upregulation of IKK signaling (e.g. phosphorylation of IκBs and Tank) which occurs more prominently in DCs infected by WT bacterium. The difference between strains becomes even more evident at 60 min p.i. when WT induces the new wave of host proteome phosphorylation. The most active components of this second signaling peak are ERK1/2-RSK1/2 and p38-MK2 kinase modules. The lower potency of Δ*dsbA* to stimulate such response represents an interesting feature of the invasion. DsbA protein is TLR2 ligand (69) but it is unlikely that its loss affected TLR-dependent MAPK activation because there is no quantitative difference in the initial signaling response of DCs to WT and Δ*dsbA*. Rather, the existence of two temporally separated

host phosphorylation waves suggests that infected DCs react to two distinct events. Considering the bacterial uptake as the origin of the initial DC response, we speculate that the second signaling wave detected at 60 min p.i. might be functionally linked to the rapid escape of WT bacteria into the cytosol. Two findings support this notion: i) only viable WT bacteria are able to trigger p38 activation and ii) while the majority of Δ*dsbA*-containing phagosomes lose their integrity at 60 min p.i., bacteria are still surrounded by vacuolar membranes and therefore not fully released. It is however impossible to conclude whether the activation of p38/ERKs at 60 min p.i. results from the enhanced cytosolic sensing of bacterial products, WT-specific rapid disruption of phagosome, or the activity of unidentified bacterial effector. In this light, it is interesting that components of cytosolic DNA-sensing pathways are not among phosphoproteins differentially regulated between WT- and Δ*dsbA*-infected DCs. It was previously shown that Δ*dsbA* of LVS background stimulates the higher production of IFN-β than its WT counterpart (70). In contrast, the expression of *Ifnb1* in DCs infected by FSC200 WT and Δ*dsbA* is lower than in LVS-infected DCs and virtually indistinguishable from uninfected cells. This suggests that the observed upregulation of MAPK signaling in WT-infected BMDCs is unrelated to STING-dependent cytosolic sensing of *Francisella* DNA (9, 10, 58, 59). The activation of MAPKs is a part of the host pro-inflammatory response and it is usually associated rather with attenuated *Francisella* strains (62, 63). For example, previous analysis of host phosphoproteome showed that p38-target tristetraproline (TPP) was phosphorylated in response to *F. novicida* Δ*lpcC* mutant and that this positively affected the stability of pro-inflammatory transcripts (63). In contrast, we observe p38-mediated TPP phosphorylation (S52; Table S1) and p38-dependent *Il12b* expression rather in DCs infected by virulent strain. These contradictory findings might be explained if we consider that the extent of MAPK activity induced by virulent *Francisella* is

assessed only relatively by the comparison with attenuated bacteria. For illustration, mutants defective in phagosomal escape are known to prolong the stimulation of TLRs from within the phagosome (7) and the comparison of these strains with WTs may lead to the conclusion that virulent *Francisella* avoids MAPK activation. Here, we employ Δ*dsbA* as a reference. The mutant is attenuated and provides protection *in vivo* (33). However, the production of IL-1β in infected DCs suggests that Δ*dsbA* probably reaches the host cytosol. Such behavior would explain the relatively low ability of Δ*dsbA* to induce TLR-dependent early MAPKs signaling when compared to phagosome-residing mutants (7). On the other hand, different kinetics of Δ*dsbA*-driven phagosomal disruption and of the cellular stress connected with the process might be responsible for the apparently high MAPKs activity WT-infected DCs at 60 min p.i. Collectively, the presented comparative study reveals that the early MAPKs signaling in *Francisella*-infected DCs is selectively engaged rather than suppressed. The preservation of mTOR activity observed at 60 min p.i. in WT-activated DCs probably helps to stimulate gene transcription and to re-configure the cell metabolism (71). Interestingly, although Akt mediated the suppression of mTOR inhibitors during the bacterial entry, mTOR activity at 60 min p.i. was partially supported by p38 (Fig. 6C) and possibly also by ERKs (66). The initial pro-inflammatory directing of WT-infected DCs is however lost in the course of *Francisella*-DC interaction and, in contrast to Δ*dsbA*-infected cells, DCs infected by virulent bacteria are not activated or matured 24 h p.i. Although the transient early activation of p38 and IκB-α phosphorylation was in *Francisella*-infected cells observed before (64), implications for bacterial virulence remain unclear. It is known that the activation of p38 helps *Francisella* to suppress the early cell death of the host (72, 73) and to downregulate MHC II (74). We propose that the positive regulation of CREB transcription factor is another side effect of p38 activation which

favors *Francisella*-mediated host survival and immunity bypass (54). It was previously shown that GSK-3β inhibition led to CREB activation and IL-10 production in LVS-infected macrophages (75). Akt-mediated inhibition of GSK-3β could be indeed responsible for CREB induction at 10 min p.i. observed in both WT- and Δ*dsbA*-infected DCs. However, phosphorylation of CREB at 60 min p.i. and the early expression of *Il10* in DCs infected by WT was p38-dependent. Although the levels of secreted IL-10 were below the limit of detection, we speculate that p38-dependently produced IL-10 may through autocrine/paracrine stimulation instruct DCs to suppress the initial inflammation and to alter the maturation (76). Taken together, our phosphoproteomic data show that the very early DC response to *Francisella* is divided into temporally separate phases which correspond to different stages of bacterial infection. We report that cytosolic virulent *Francisella* induces MAPKs and early gene expression and that these processes are the earliest events regulated differentially in DCs infected by WT and attenuated Δ*dsbA* strains of fully virulent FSC200 bacterial background. The temporal orchestration of host pro-inflammatory pathways therefore represents the integral part of *Francisella* life-cycle inside hijacked DCs. In this regard, the detailed analysis of early-intermediate gene expression in cells exposed to the bacterium may provide new insights into how DCs acquire their unproductive phenotype.

References

1. Kubelkova, K., and Macela, A. (2015) Putting the Jigsaw Together - A Brief Insight Into the Tularemia. *Open Life Sci.* 10,

2. Oyston, P. C. F., Sjostedt, A., and Titball, R. W. (2004) Tularaemia: bioterrorism defence renews interest in *Francisella tularensis*. *Nat. Rev. Microbiol.* 2, 967–978

3. Sharma, J., Mares, C. A., Li, Q., Morris, E. G., and Teale, J. M. (2011) Features of sepsis caused by pulmonary infection with *Francisella tularensis* Type A strain. *Microb. Pathog.* 51, 39–47

4. Asare, R., and Kwaik, Y. A. (2010) Exploitation of host cell biology and evasion of immunity by *Francisella tularensis*. *Front. Microbiol.* 1, 145

5. Santic, M., Al-Khodor, S., and Abu Kwaik, Y. (2010) Cell biology and molecular ecology of *Francisella tularensis*. *Cell. Microbiol.* 12, 129–139

6. Fabrik, I., Härtlova, A., Rehulka, P., and Stulik, J. (2013) Serving the new masters - dendritic cells as hosts for stealth intracellular bacteria. *Cell. Microbiol.* 15, 1473–1483

7. Cole, L. E., Santiago, A., Barry, E., Kang, T. J., Shirey, K. A., Roberts, Z. J., Elkins, K. L., Cross, A. S., and Vogel, S. N. (2008) Macrophage proinflammatory response to *Francisella tularensis* live vaccine strain requires coordination of multiple signaling pathways. *J. Immunol. Baltim. Md 1950* 180, 6885–6891

8. Cremer, T. J., Butchar, J. P., and Tridandapani, S. (2011) *Francisella* Subverts Innate Immune Signaling: Focus On PI3K/Akt. *Front. Microbiol.* 5, 13

9. Storek, K. M., Gertsvolf, N. A., Ohlson, M. B., and Monack, D. M. (2015) cGAS and Ifi204 cooperate to produce type I IFNs in response to *Francisella* infection. *J. Immunol. Baltim. Md 1950* 194, 3236–3245

10. Jones, J. W., Kayagaki, N., Broz, P., Henry, T., Newton, K., O'Rourke, K., Chan, S., Dong, J., Qu, Y., Roose-Girma, M., Dixit, V. M., and Monack, D. M. (2010) Absent in melanoma 2 is required for innate immune recognition of *Francisella tularensis*. *Proc. Natl. Acad. Sci. U. S. A.* 107, 9771–9776

11. Bauler, T. J., Chase, J. C., and Bosio, C. M. (2011) IFN-β mediates suppression of IL-12p40 in human dendritic cells following infection with virulent *Francisella tularensis*. *J. Immunol. Baltim. Md 1950* 187, 1845–1855

12. Fabrik, I., Link, M., Härtlova, A., Dankova, V., Rehulka, P., and Stulik, J. (2014) Application of SILAC labeling to primary bone marrow-derived dendritic cells reveals extensive GM-CSF-dependent arginine metabolism. *J. Proteome Res.* 13, 752–762

13. Rogers, L. D., Fang, Y., and Foster, L. J. (2010) An integrated global strategy for cell lysis, fractionation, enrichment and mass spectrometric analysis of phosphorylated peptides. *Mol. Biosyst.* 6, 822–829

14. Yeung, Y.-G., and Stanley, E. R. (2010) Rapid detergent removal from peptide samples with ethyl acetate for mass spectrometry analysis. *Curr. Protoc. Protein Sci.* Chapter 16, Unit 16.12

15. McNulty, D. E., and Annan, R. S. (2008) Hydrophilic interaction chromatography reduces the complexity of the phosphoproteome and improves global phosphopeptide isolation and detection. *Mol. Cell. Proteomics MCP* 7, 971–980

16. Härtlova, A., Link, M., Balounova, J., Benesova, M., Resch, U., Straskova, A., Sobol, M., Philimonenko, A., Hozak, P., Krocova, Z., Gekara, N., Filipp, D., and Stulik, J. (2014) Quantitative proteomics analysis of macrophage-derived lipid rafts reveals induction of autophagy pathway at the early time of *Francisella tularensis* LVS infection. *J. Proteome Res.* 13, 796–804

17. Michalski, A., Damoc, E., Hauschild, J.-P., Lange, O., Wieghaus, A., Makarov, A., Nagaraj, N., Cox, J., Mann, M., and Horning, S. (2011) Mass spectrometry-based proteomics using Q Exactive, a high-performance benchtop quadrupole Orbitrap mass spectrometer. *Mol. Cell. Proteomics MCP* 10, M111.011015

18. Cox, J., and Mann, M. (2008) MaxQuant enables high peptide identification rates, individualized p.p.b.-range mass accuracies and proteome-wide protein quantification. *Nat. Biotechnol.* 26, 1367–1372

19. Klammer, M., Dybowski, J. N., Hoffmann, D., and Schaab, C. (2014) Identification of significant features by the Global Mean Rank test. *PloS One* 9, e104504

20. Zhou, Y., Cras-Méneur, C., Ohsugi, M., Stormo, G. D., and Permutt, M. A. (2007) A global approach to identify differentially expressed genes in cDNA (two-color) microarray experiments. *Bioinforma. Oxf. Engl.* 23, 2073–2079

21. Futschik, M. E., and Carlisle, B. (2005) Noise-robust soft clustering of gene expression time-course data. *J. Bioinform. Comput. Biol.* 3, 965–988

22. Olsen, J. V., Blagoev, B., Gnad, F., Macek, B., Kumar, C., Mortensen, P., and Mann, M. (2006) Global, *in vivo*, and site-specific phosphorylation dynamics in signaling networks. *Cell* 127, 635–648

23. Sharma, K., D'Souza, R. C. J., Tyanova, S., Schaab, C., Wiśniewski, J. R., Cox, J., and Mann, M. (2014) Ultradeep human phosphoproteome reveals a distinct regulatory nature of Tyr and Ser/Thr-based signaling. *Cell Rep.* 8, 1583–1594

24. Kumar, L., and E Futschik, M. (2007) Mfuzz: a software package for soft clustering of microarray data. *Bioinformation* 2, 5–7

25. Schwämmle, V., and Jensen, O. N. (2010) A simple and fast method to determine the parameters for fuzzy *c*-means cluster analysis. *Bioinforma. Oxf. Engl.* 26, 2841–2848

26. Keshava Prasad, T. S., Goel, R., Kandasamy, K., Keerthikumar, S., Kumar, S., Mathivanan, S., Telikicherla, D., Raju, R., Shafreen, B., Venugopal, A., Balakrishnan, L., Marimuthu, A., Banerjee, S., Somanathan, D. S., Sebastian, A., Rani, S., Ray, S., Harrys Kishore, C. J., Kanth, S., Ahmed, M., Kashyap, M. K., Mohmood, R., Ramachandra, Y. L., Krishna, V., Rahiman, B. A., Mohan, S., Ranganathan, P., Ramabadran, S., Chaerkady, R., and Pandey, A. (2009) Human Protein Reference Database--2009 update. *Nucleic Acids Res.* 37, D767-772

27. Tyanova, S., Temu, T., Sinitcyn, P., Carlson, A., Hein, M. Y., Geiger, T., Mann, M., and Cox, J. (2016) The Perseus computational platform for comprehensive analysis of (prote)omics data. *Nat. Methods* 13, 731–740

28. Breuer, K., Foroushani, A. K., Laird, M. R., Chen, C., Sribnaia, A., Lo, R., Winsor, G. L., Hancock, R. E. W., Brinkman, F. S. L., and Lynn, D. J. (2013) InnateDB: systems biology of innate immunity and beyond--recent updates and continuing curation. *Nucleic Acids Res.* 41, D1228-1233

29. Szklarczyk, D., Franceschini, A., Wyder, S., Forslund, K., Heller, D., Huerta-Cepas, J., Simonovic, M., Roth, A., Santos, A., Tsafou, K. P., Kuhn, M., Bork, P., Jensen, L. J., and von Mering, C. (2015) STRING v10: protein-protein interaction networks, integrated over the tree of life. *Nucleic Acids Res.* 43, D447-452

30. Kim, H. G., Kim, J. Y., Gim, M. G., Lee, J. M., and Chung, D. K. (2008) Mechanical stress induces tumor necrosis factor-α production through Ca^{2+} release-dependent TLR2 signaling. *Am. J. Physiol. Cell Physiol.* 295, C432-439

31. Qin, A., Scott, D. W., Thompson, J. A., and Mann, B. J. (2009) Identification of an essential *Francisella tularensis* subsp. *tularensis* virulence factor. *Infect. Immun.* 77, 152–161

32. Straskova, A., Pavkova, I., Link, M., Forslund, A.-L., Kuoppa, K., Noppa, L., Kroca, M., Fucikova, A., Klimentova, J., Krocova, Z., Forsberg, A., and Stulik, J. (2009) Proteome analysis of an attenuated *Francisella tularensis dsbA* mutant: identification of potential DsbA substrate proteins. *J. Proteome Res.* 8, 5336–5346

33. Straskova, A., Spidlova, P., Mou, S., Worsham, P., Putzova, D., Pavkova, I., and Stulik, J. (2015) *Francisella tularensis* type B Δ*dsbA* mutant protects against type A strain and induces strong inflammatory cytokine and Th1-like antibody response *in vivo*. *Pathog. Dis.* 73, ftv058

34. Straskova, A., Cerveny, L., Spidlova, P., Dankova, V., Belcic, D., Santic, M., and Stulik, J. (2012) Deletion of IglH in virulent *Francisella tularensis* subsp. *holarctica* FSC200 strain results in attenuation and provides protection against the challenge with the parental strain. *Microbes Infect.* 14, 177–187

35. Hashimoto, M., Sagara, Y., Langford, D., Everall, I. P., Mallory, M., Everson, A., Digicaylioglu, M., and Masliah, E. (2002) Fibroblast growth factor 1 regulates signaling via the glycogen synthase kinase-3β pathway. Implications for neuroprotection. *J. Biol. Chem.* 277, 32985–32991

36. Manning, B. D., Tee, A. R., Logsdon, M. N., Blenis, J., and Cantley, L. C. (2002) Identification of the tuberous sclerosis complex-2 tumor suppressor gene product tuberin as a target of the phosphoinositide 3-kinase/akt pathway. *Mol. Cell* 10, 151–162

37. Ning, J., Xi, G., and Clemmons, D. R. (2011) Suppression of AMPK activation via S485 phosphorylation by IGF-I during hyperglycemia is mediated by AKT activation in vascular smooth muscle cells. *Endocrinology* 152, 3143–3154

38. Vander Haar, E., Lee, S.-I., Bandhakavi, S., Griffin, T. J., and Kim, D.-H. (2007) Insulin signalling to mTOR mediated by the Akt/PKB substrate PRAS40. *Nat. Cell Biol.* 9, 316–323

39. Acosta-Jaquez, H. A., Keller, J. A., Foster, K. G., Ekim, B., Soliman, G. A., Feener, E. P., Ballif, B. A., and Fingar, D. C. (2009) Site-specific mTOR phosphorylation promotes mTORC1-mediated signaling and cell growth. *Mol. Cell. Biol.* 29, 4308–4324

40. Kim, Y.-M., Stone, M., Hwang, T. H., Kim, Y.-G., Dunlevy, J. R., Griffin, T. J., and Kim, D.-H. (2012) SH3BP4 is a negative regulator of amino acid-Rag GTPase-mTORC1 signaling. *Mol. Cell* 46, 833–846

41. Dalby, K. N., Morrice, N., Caudwell, F. B., Avruch, J., and Cohen, P. (1998) Identification of regulatory phosphorylation sites in mitogen-activated protein kinase (MAPK)-activated protein kinase-1a/p90rsk that are inducible by MAPK. *J. Biol. Chem.* 273, 1496–1505

42. Kang, S., Dong, S., Gu, T.-L., Guo, A., Cohen, M. S., Lonial, S., Khoury, H. J., Fabbro, D., Gilliland, D. G., Bergsagel, P. L., Taunton, J., Polakiewicz, R. D., and Chen, J. (2007) FGFR3 activates RSK2 to mediate hematopoietic transformation through tyrosine phosphorylation of RSK2 and activation of the MEK/ERK pathway. *Cancer Cell* 12, 201–214

43. Engel, K., Schultz, H., Martin, F., Kotlyarov, A., Plath, K., Hahn, M., Heinemann, U., and Gaestel, M. (1995) Constitutive activation of mitogen-activated protein kinase-activated protein kinase 2 by mutation of phosphorylation sites and an A-helix motif. *J. Biol. Chem.* 270, 27213–27221

44. Tomás-Zuber, M., Mary, J. L., Lamour, F., Bur, D., and Lesslauer, W. (2001) C-terminal elements control location, activation threshold, and p38 docking of ribosomal S6 kinase B (RSKB). *J. Biol. Chem.* 276, 5892–5899

45. Matsuura, H., Nishitoh, H., Takeda, K., Matsuzawa, A., Amagasa, T., Ito, M., Yoshioka, K., and Ichijo, H. (2002) Phosphorylation-dependent scaffolding role of JSAP1/JIP3 in the ASK1-JNK signaling pathway. A new mode of regulation of the MAP kinase cascade. *J. Biol. Chem.* 277, 40703–40709

46. Santic, M., Asare, R., Skrobonja, I., Jones, S., and Abu Kwaik, Y. (2008) Acquisition of the vacuolar ATPase proton pump and phagosome acidification are essential for escape of *Francisella tularensis* into the macrophage cytosol. *Infect. Immun.* 76, 2671–2677

47. Chong, A., Wehrly, T. D., Nair, V., Fischer, E. R., Barker, J. R., Klose, K. E., and Celli, J. (2008) The early phagosomal stage of *Francisella tularensis* determines optimal phagosomal escape and *Francisella* pathogenicity island protein expression. *Infect. Immun.* 76, 5488–5499

48. Clark, K., Peggie, M., Plater, L., Sorcek, R. J., Young, E. R. R., Madwed, J. B., Hough, J., McIver, E. G., and Cohen, P. (2011) Novel cross-talk within the IKK family controls innate immunity. *Biochem. J.* 434, 93–104

49. Shirane, M., Hatakeyama, S., Hattori, K., Nakayama, K., and Nakayama, K. (1999) Common pathway for the ubiquitination of IκBα, IκBβ, and IκBε mediated by the F-box protein FWD1. *J. Biol. Chem.* 274, 28169–28174

50. Leotoing, L., Chereau, F., Baron, S., Hube, F., Valencia, H. J., Bordereaux, D., Demmers, J. A., Strouboulis, J., and Baud, V. (2011) A20-binding inhibitor of nuclear factor-κB (NF-κB)-2 (ABIN-2) is an activator of inhibitor of NF-κB (IκB) kinase α (IKKα)-mediated NF-κB transcriptional activity. *J. Biol. Chem.* 286, 32277–32288

51. Sanjabi, S., Hoffmann, A., Liou, H. C., Baltimore, D., and Smale, S. T. (2000) Selective requirement for c-Rel during IL-12 P40 gene induction in macrophages. *Proc. Natl. Acad. Sci. U. S. A.* 97, 12705–12710

52. Zhu, C., Gagnidze, K., Gemberling, J. H., and Plevy, S. E. (2001) Characterization of an activation protein-1-binding site in the murine interleukin-12 p40 promoter. Demonstration of novel functional elements by a reductionist approach. *J. Biol. Chem.* 276, 18519–18528

53. Olson, C. M., Hedrick, M. N., Izadi, H., Bates, T. C., Olivera, E. R., and Anguita, J. (2007) p38 mitogen-activated protein kinase controls NF-κB transcriptional activation and tumor necrosis factor alpha production through RelA phosphorylation mediated by mitogen- and stress-activated protein kinase 1 in response to *Borrelia burgdorferi* antigens. *Infect. Immun.* 75, 270–277

54. Wen, A. Y., Sakamoto, K. M., and Miller, L. S. (2010) The role of the transcription factor CREB in immune function. *J. Immunol. Baltim. Md 1950* 185, 6413–6419

55. Screaton, R. A., Conkright, M. D., Katoh, Y., Best, J. L., Canettieri, G., Jeffries, S., Guzman, E., Niessen, S., Yates, J. R., Takemori, H., Okamoto, M., and Montminy, M. (2004) The CREB coactivator TORC2 functions as a calcium- and cAMP-sensitive coincidence detector. *Cell* 119, 61–74

56. Tan, Y., Rouse, J., Zhang, A., Cariati, S., Cohen, P., and Comb, M. J. (1996) FGF and stress regulate CREB and ATF-1 via a pathway involving p38 MAP kinase and MAPKAP kinase-2. *EMBO J.* 15, 4629–4642

57. Deak, M., Clifton, A. D., Lucocq, L. M., and Alessi, D. R. (1998) Mitogen- and stress-activated protein kinase-1 (MSK1) is directly activated by MAPK and SAPK2/p38, and may mediate activation of CREB. *EMBO J.* 17, 4426–4441

58. Tanaka, Y., and Chen, Z. J. (2012) STING specifies IRF3 phosphorylation by TBK1 in the cytosolic DNA signaling pathway. *Sci. Signal.* 5, ra20

59. Henry, T., Brotcke, A., Weiss, D. S., Thompson, L. J., and Monack, D. M. (2007) Type I interferon signaling is required for activation of the inflammasome during *Francisella* infection. *J. Exp. Med.* 204, 987–994

60. Mashima, R., Saeki, K., Aki, D., Minoda, Y., Takaki, H., Sanada, T., Kobayashi, T., Aburatani, H., Yamanashi, Y., and Yoshimura, A. (2005) FLN29, a novel interferon- and LPS-inducible gene acting as a negative regulator of toll-like receptor signaling. *J. Biol. Chem.* 280, 41289–41297

61. Sanada, T., Takaesu, G., Mashima, R., Yoshida, R., Kobayashi, T., and Yoshimura, A. (2008) FLN29 deficiency reveals its negative regulatory role in the Toll-like receptor (TLR) and retinoic acid-inducible gene I (RIG-I)-like helicase signaling pathway. *J. Biol. Chem.* 283, 33858–33864

62. Huang, M. T.-H., Mortensen, B. L., Taxman, D. J., Craven, R. R., Taft-Benz, S., Kijek, T. M., Fuller, J. R., Davis, B. K., Allen, I. C., Brickey, W. J., Gris, D., Wen, H., Kawula, T. H., and Ting, J. P.-Y. (2010) Deletion of *ripA* alleviates suppression of the inflammasome and MAPK by *Francisella tularensis*. *J. Immunol. Baltim. Md 1950* 185, 5476–5485

63. Nakayasu, E. S., Tempel, R., Cambronne, X. A., Petyuk, V. A., Jones, M. B., Gritsenko, M. A., Monroe, M. E., Yang, F., Smith, R. D., Adkins, J. N., and Heffron, F. (2013) Comparative phosphoproteomics reveals components of host cell invasion and post-transcriptional regulation during *Francisella* infection. *Mol. Cell. Proteomics MCP* 12, 3297–3309

64. Telepnev, M., Golovliov, I., and Sjöstedt, A. (2005) *Francisella tularensis* LVS initially activates but subsequently down-regulates intracellular signaling and cytokine secretion in mouse monocytic and human peripheral blood mononuclear cells. *Microb. Pathog.* 38, 239–247

65. Parsa, K. V. L., Butchar, J. P., Rajaram, M. V. S., Cremer, T. J., and Tridandapani, S. (2008) The tyrosine kinase Syk promotes phagocytosis of *Francisella* through the activation of Erk. *Mol. Immunol.* 45, 3012–3021

66. Edwards, M. W., Aultman, J. A., Harber, G., Bhatt, J. M., Sztul, E., Xu, Q., Zhang, P., Michalek, S. M., and Katz, J. (2013) Role of mTOR downstream effector signaling molecules in *Francisella tularensis* internalization by murine macrophages. *PloS One* 8, e83226

67. Van den Broeke, C., Radu, M., Chernoff, J., and Favoreel, H. W. (2010) An emerging role for p21-activated kinases (Paks) in viral infections. *Trends Cell Biol.* 20, 160–169

68. Moreau, G. B., and Mann, B. J. (2013) Adherence and uptake of *Francisella* into host cells. *Virulence* 4, 826–832

69. Thakran, S., Li, H., Lavine, C. L., Miller, M. A., Bina, J. E., Bina, X. R., and Re, F. (2008) Identification of *Francisella tularensis* lipoproteins that stimulate the toll-like receptor (TLR) 2/TLR1 heterodimer. *J. Biol. Chem.* 283, 3751–3760

70. Putzova, D., Panda, S., Härtlova, A., Stulík, J., and Gekara, N. O. (2017) Subversion of innate immune responses by *Francisella* involves the disruption of TRAF3 and TRAF6 signalling complexes. *Cell. Microbiol.*, doi: 10.1111/cmi.12769

71. Sukhbaatar, N., Hengstschläger, M., and Weichhart, T. (2016) mTOR-Mediated Regulation of Dendritic Cell Differentiation and Function. *Trends Immunol.* 37, 778–789

72. Hrstka, R., Stulík, J., and Vojtesek, B. (2005) The role of MAPK signal pathways during *Francisella tularensis* LVS infection-induced apoptosis in murine macrophages. *Microbes Infect.* 7, 619–625

73. Santic, M., Pavokovic, G., Jones, S., Asare, R., and Kwaik, Y. A. (2010) Regulation of apoptosis and anti-apoptosis signalling by *Francisella tularensis*. *Microbes Infect.* 12, 126–134

74. Brummett, A. M., Navratil, A. R., Bryan, J. D., and Woolard, M. D. (2014) Janus kinase 3 activity is necessary for phosphorylation of cytosolic phospholipase A2 and prostaglandin E2 synthesis by macrophages infected with *Francisella tularensis* live vaccine strain. *Infect. Immun.* 82, 970–982

75. Zhang, P., Katz, J., and Michalek, S. M. (2009) Glycogen synthase kinase-3β (GSK3β) inhibition suppresses the inflammatory response to *Francisella* infection and protects against tularemia in mice. *Mol. Immunol.* 46, 677–687

76. Corinti, S., Albanesi, C., la Sala, A., Pastore, S., and Girolomoni, G. (2001) Regulatory activity of autocrine IL-10 on dendritic cell functions. *J. Immunol. Baltim. Md 1950* 166, 4312–4318

Acknowledgments: We thank prof. Yousef Abu Kwaik for critical reading of the manuscript and Jitka Zakova and Lenka Luksikova (University of Defence) for excellent technical assistance. The authors have declared no conflict of interests.

Funding: The work was supported by the Czech Science Foundation (15-02584S). Marina Santic was supported by the Croatian Science Foundation (HRZZZ-9003). The Microscopy Centre − Electron Microscopy CF, IMG AS CR is supported by the Czech-BioImaging large RI project (LM2015062 funded by MEYS CR) and by OP RDE (CZ.02.1.01/0.0/0.0/16_013/0001775).

Data availability: Proteomics data were deposited to the ProteomeXchange Consortium (http://proteomecentral.proteomexchange.org) via the PRIDE partner repository with the dataset identifiers PXD005747 (phosphoproteome) and PXD006759 (proteome) and MS/MS spectra can be viewed on MS-Viewer (http://msviewer.ucsf.edu/prospector/cgi-bin/msform.cgi?form=msviewer) using the search keys uomohcoiy9 (phosphoproteome) and oqiga3hn5r (proteome).

Figure Legends:

Fig. 1: Protein phosphorylation induced in BMDCs during the first hour of infection by *Francisella tularensis* subsp. *holarctica* FSC200 (WT) strain. SILAC-labeled BMDCs were infected with WT (MOI 50) for 10, 30 or 60 min (Fig. S1) and processed as described in Experimental procedures. (**A**) Histograms of normalized SILAC log_2-ratios (Mock/WT) of phosphosites from infected BMDCs. Data collected from means of three biological replicates with RSD <30%. (**B**) Count of significantly regulated phosphosites per given time p.i. (Global Mean Rank Test, FDR <0.05). (**C**) Count of phosphosites which were assigned to fuzzy *c*-means clusters. (**D**) Fuzzy *c*-means clustered phosphosites from infected BMDCs. (**E**) Western blot analysis of selected kinases. Data are representative from biological duplicate.

Fig. 2: *Francisella* Δ*dsbA* mutant stimulates *in vitro* BMDC activation and maturation. BMDCs were infected by FSC200 WT, FSC200 Δ*dsbA* or LVS at MOI 10 or treated by *E. coli* LPS (500 ng/ml) and left for 24 hours. (**A**) Flow cytometric analysis of cell surface expression of MHC II, CD80 and CD86. Histograms are representative from biological triplicate. (**B**) Concentrations of IL-12p40, IL-1β and IL-6 in culture supernatants were determined by ELISA. Data are presented as means ± SEM of independent replicates; n = 3; **p* <0.05 (Student's t test). (**C**) Electron micrographs of BMDCs infected by WT and Δ*dsbA* at 60 min p.i. (MOI 50). Black arrow shows free bacteria in the cytosol. White arrow indicates the damaged phagosomal membrane. Lengths of scale bars are 0.2 μm and 0.1 μm for micrographs showing WT and Δ*dsbA*, respectively. Data are representative from biological triplicate.

Fig. 3: BMDCs infected by WT maintain mTOR/p70S6K signaling at 60 min p.i. (**A**) Time-dependent changes in phosphorylation of known Akt targets in WT- and Δ*dsbA*-infected BMDCs. (**B**) Time-dependent site phosphorylation in proteins connected to mTOR localization to lysosome – all sites were significantly upregulated at 60 min p.i. only in WT-infected BMDCs (Global Mean Rank Test, FDR <0.05). Bar graphs show the situation at 60 min p.i. for sites quantified only at this time point. Headings of graphs in (**A**) and (**B**) contain gene name/protein name, Uniprot accession number and phosphosite position. SILAC-based phosphorylation changes are expressed as a mean ± SEM (n = 3) of normalized fold change (FC, infected/mock) at respective time p.i.; **p* <0.05 (Student's t test applied on normalized SILAC $\log_2$-ratios). In graphs, "C" designates no change (FC = 1) and up- and downregulated phosphosites are represented by positive and negative FC values, respectively. (**C**) Western blot analysis of phosphosites connected to mTOR activity in infected BMDCs. Data are representative from biological duplicate.

Fig. 4: Signaling in BMDCs infected by WT and Δ*dsbA* starts to diverge at 60 min p.i. (**A**) Means of normalized $\log_2$-ratios of phosphosites quantified in all three biological replicates of SILAC experiment with RSD <30% per given time p.i. in WT-infected BMDCs were correlated with the corresponding values of the same site in Δ*dsbA*-infected cells. Black line represents x = y function, red line shows the actual correlation with Pearson coefficient (*r*) for the given time p.i. (**B**) Innate DB terms enriched in the group of proteins differentially phosphorylated in WT- and Δ*dsbA*-infected BMDCs at 60 min p.i. (Fisher exact test; BH FDR <0.05). Only those terms containing at least 3 differentially regulated phosphosites are presented.

Fig. 5: ERK and p38 modules are induced in WT-infected BMDCs at 60 min p.i. (**A**) Protein-protein interaction network constructed on STRING background containing 80 proteins differentially phosphorylated in WT- and Δ*dsbA*-infected BMDCs at 60 min p.i. (large circles). Magnified part shows MAPK interaction cluster. The color of large circles corresponds to the absolute value of the difference between means of phosphosite normalized SILAC $\log_2$-ratios in WT- and Δ*dsbA*-infected BMDCs at 60 min p.i. The whole network is in Fig. S8. For details see Experimental procedures. (**B**) Time-dependent and (**C**) 60 min p.i. changes in phosphorylation of MAPK-connected phosphosites in WT- and Δ*dsbA*-infected BMDCs. See Fig. 3 legend for the description of the graphs. (**D**) Western blot analysis of phosphosites connected to MAPKs activity in infected BMDCs. Data are representative from biological duplicate.

Fig. 6: p38-regulates the gene expression in WT-infected BMDCs. (**A**) Time-dependent changes in phosphorylation of selected phosphosites in WT- and Δ*dsbA*-infected BMDCs. (**B**) Phosphorylation of IκB-α and CREB in WT- and Δ*dsbA*-infected BMDCs (MOI 50) during the first hour of infection. (**C**) Phosphorylation of Jun, CREB and p70S6K in WT-infected BMDCs at 60 min p.i. Cells were pre-treated either by DMSO or p38-inhibitor SB203580 for 60 min prior to infection. (**D**) Stable expression of *Il12b* and *Il10* mRNA in WT- and Δ*dsbA*-infected BMDCs (MOI 50) and in mock-treated cells during 4 h p.i. (**E**) Stable expression of *Il12b* and *Il10* mRNA at 2 h p.i. in WT-infected BMDCs. Cells were pre-treated either by DMSO or p38-inhibitor SB203580 for 60 min prior to infection. (**F**) A model of phosphorylation-mediated early DC signaling in response to infection by *Francisella tularensis* subsp. *holarctica* FSC200. For

the description of graphs in (**A**), see Fig. 3 legend. The changes in mRNA transcription in (**D**) and (**E**) are expressed as a mean ± SEM (n = 3) FC (infected over mock left for 1 h); **p* <0.05 (Student's t test applied on ΔΔCt values from WT- and Δ*dsbA*-infected BMDCs). In graphs, "C" designates no change (FC = 1). Western blots are representative from biological duplicates.

Tables:

Table 1: HPRD motifs enriched in phosphosite clusters from Fig. 1D. Motifs were found by Fisher exact test (BH FDR <0.05). Only those with enrichment factor >1.2 are presented. None motif was found for cluster C.

Cluster	HPRD motif	Enrichment factor	FDR
A	p70 Ribosomal S6 kinase	2.33	3.02×10^{-7}
	Aurora-A kinase	1.97	6.82×10^{-4}
	Phosphorylase kinase	1.64	1.50×10^{-5}
	Akt kinase	1.57	3.82×10^{-4}
	MAPKAPK1 kinase	1.55	2.39×10^{-4}
	PAK2 kinase	1.53	2.65×10^{-3}
	PKC epsilon kinase	1.46	6.21×10^{-3}
	MAPKAPK2 kinase	1.30	7.85×10^{-3}
	14-3-3 domain binding motif	1.27	2.05×10^{-4}
	Calmodulin-dependent protein kinase II	1.21	1.30×10^{-3}
B	Growth associated histone HI kinase	1.48	2.38×10^{-3}
	ERK1,2 kinase	1.26	7.96×10^{-5}
	WW domain binding motif	1.21	3.31×10^{-4}
	GSK-3, ERK1, ERK2, CDK5	1.21	3.68×10^{-4}
D	Calmodulin-dependent protein kinase I	2.10	1.14×10^{-2}
	AMP-activated protein kinase	1.70	1.49×10^{-2}

Fig. 1

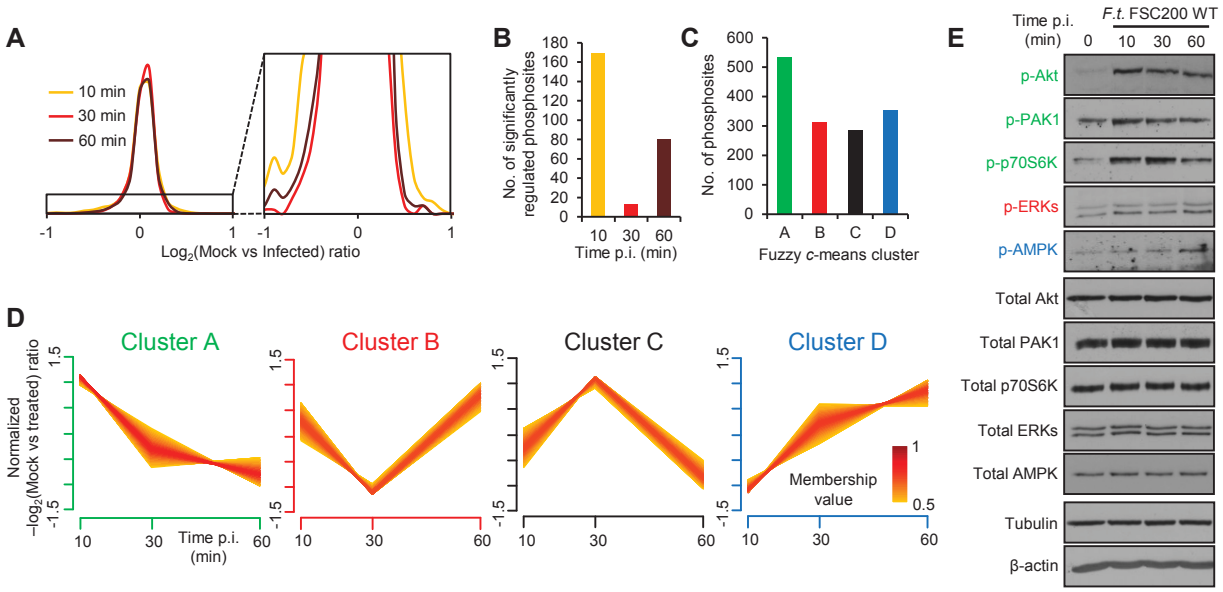

Fig. 2

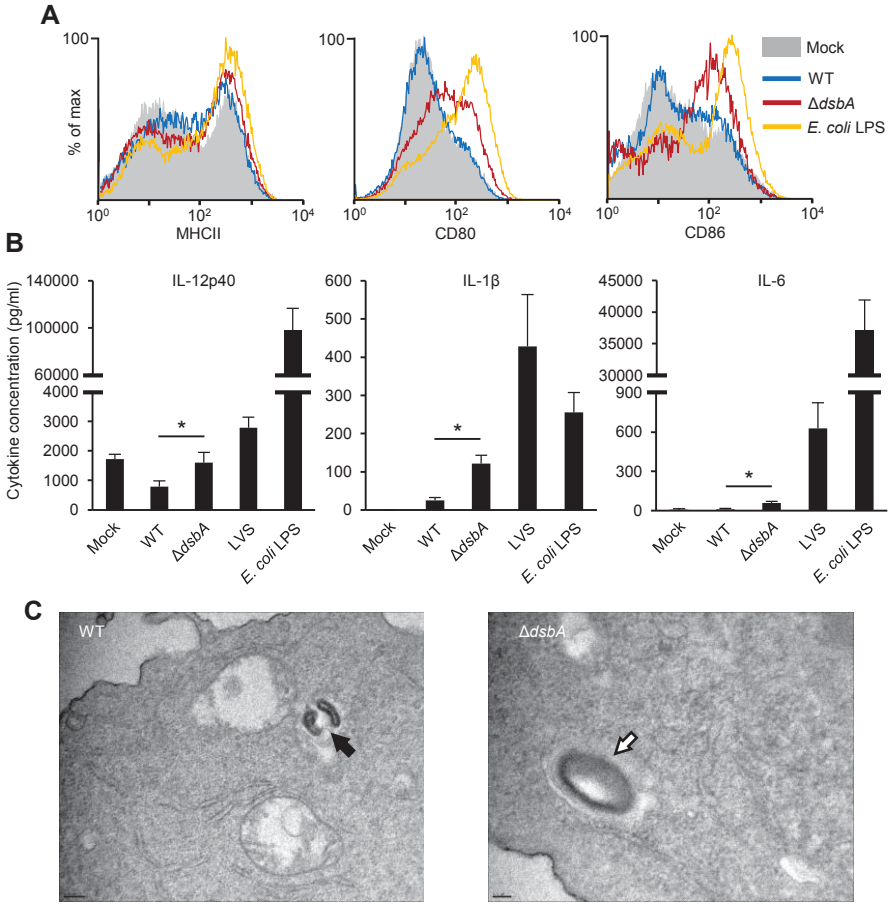

Fig. 3

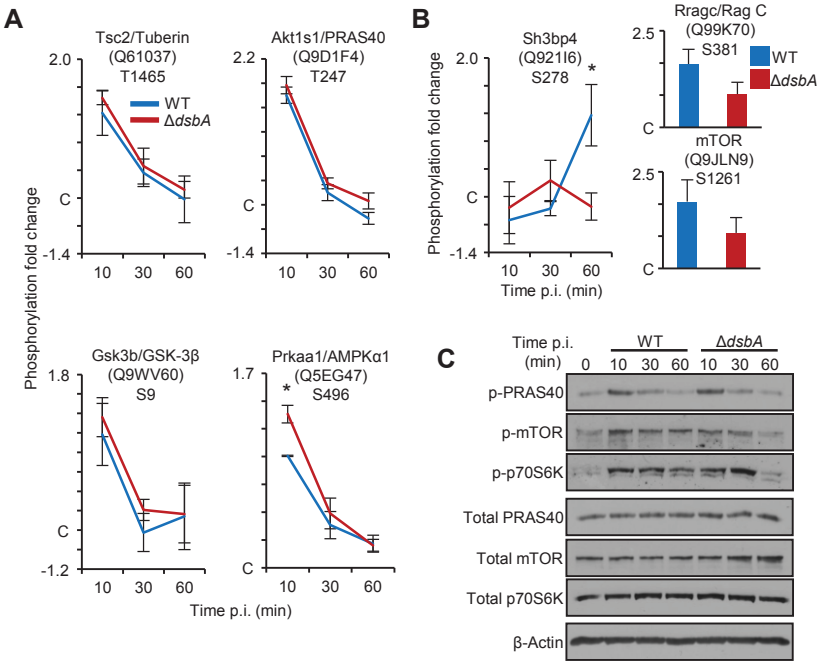

Fig. 4

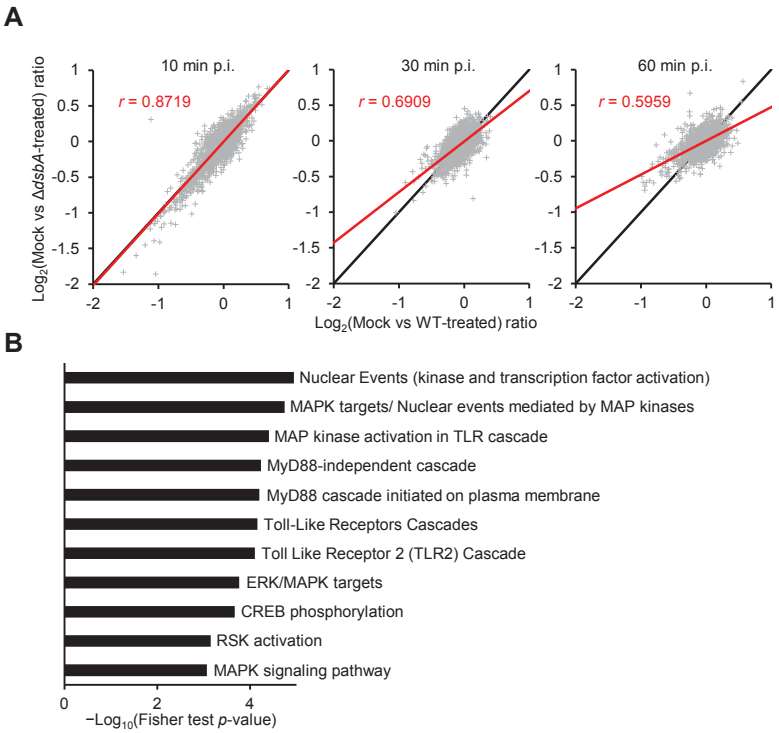

Fig. 5

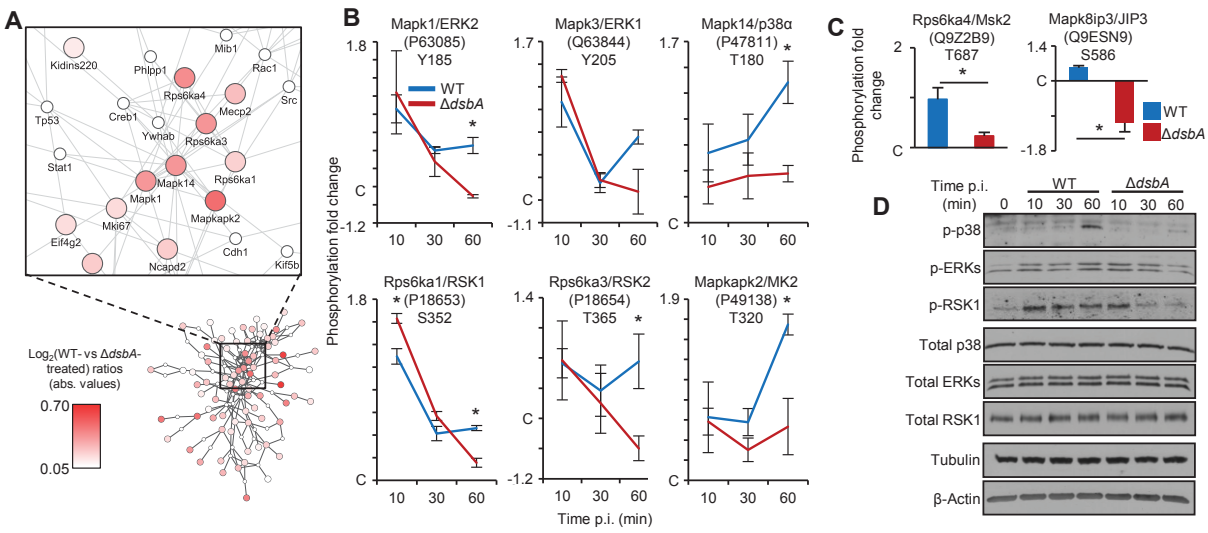

Fig. 6